Network structure and local adaptation in co-evolving bacteria–phage interactions

JAMES GURNEY,* LAFI ALDAKAK,* ALEX BETTS,† CLAIRE GOUGAT-BARBERA,*
TIMOTHÉE POISOT,‡ OLIVER KALTZ*[1] (iD) and MICHAEL E. HOCHBERG*§[1] (iD)
*Institut des Sciences de l'Evolution de Montpellier, UMR5554, Université de Montpellier, CC065, Place E. Bataillon,
34095 Montpellier Cedex 5, France, †Department of Zoology, University of Oxford, Oxford OX1 3PS, UK, ‡Département de
Sciences Biologiques, Université de Montréal, Pavillon Marie-Victorin, 90, avenue Vincent-d'Indy, Montréal H2V 2S9, Canada,
§Santa Fe Institute, 1399 Hyde Park Rd., Santa Fe, NM 87501, USA

Abstract

Numerous theoretical and experimental studies have investigated antagonistic co-evolution between parasites and their hosts. Although experimental tests of theory from a range of biological systems are largely concordant regarding the influence of several driving processes, we know little as to how mechanisms acting at the smallest scales (individual molecular and phenotypic changes) may result in the emergence of structures at larger scales, such as co-evolutionary dynamics and local adaptation. We capitalized on methods commonly employed in community ecology to quantify how the structure of community interaction matrices, so-called bipartite networks, reflected observed co-evolutionary dynamics, and how phages from these communities may or may not have adapted locally to their bacterial hosts. We found a consistent nested network structure for two phage types, one previously demonstrated to exhibit arms race co-evolutionary dynamics and the other fluctuating co-evolutionary dynamics. Both phages increased their host ranges through evolutionary time, but we found no evidence for a trade-off with impact on bacteria. Finally, only bacteria from the arms race phage showed local adaptation, and we provide preliminary evidence that these bacteria underwent (sometimes different) molecular changes in the *wzy* gene associated with the LPS receptor, while bacteria co-evolving with the fluctuating selection phage did not show local adaptation and had partial deletions of the *pilF* gene associated with type IV pili. We conclude that the structure of phage–bacteria interaction networks is not necessarily specific to co-evolutionary dynamics, and discuss hypotheses for why only one of the two phages was, nevertheless, locally adapted.

Keywords: bacteria, bacteriophage, bipartite networks, co-evolution, experimental evolution, local adaptation

Received 30 September 2016; revision received 16 December 2016; accepted 19 December 2016

Introduction

Dynamic populations of enemies, such as parasites or predators, are thought to impose constantly changing selection pressures on their victims (hosts or prey). In combination with environmental variation, these interactions drive genetic population diversification and adaptive responses. A large body of theoretical work on the most studied form of antagonistic co-evolution, between hosts and their parasites, has provided a conceptual framework of how parasite exploitation and host resistance traits interact and change over evolutionary time, and how co-evolutionary trajectories depend on underlying interaction genetics, trade-offs between interaction traits and life history traits, reproductive systems, migration in patchy habitats or

Correspondence: Michael E. Hochberg, ISEM, CNRS-Université de Montpellier, CC065, Place E. Bataillon, Montpellier 34095, France, Fax: +33 (0)4 67 14 36 22; E-mail: mhochber@univ-montp2.fr
[1]Equal contribution.

environmental heterogeneity (e.g. Bell *et al.* 1987; Hochberg & Holt 1995; Gandon *et al.* 1996; Hochberg & Baalen 1998; Thompson 1999; Gomulkiewicz *et al.* 2000; Agrawal & Lively 2002; Poisot *et al.* 2011a; Ashby *et al.* 2014). Many of the predictions emerging from this theory have been tested in the laboratory (e.g. Forde *et al.* 2004; Fischer & Schmid-Hempel 2005; Lopez-Pascua & Buckling 2008; Hall *et al.* 2011b; Koskella *et al.* 2011; Friman & Buckling 2013; Harrison *et al.* 2013; Koskella & Brockhurst 2014; Gómez *et al.* 2015) and field (Dybdahl & Lively 1998; Kaltz *et al.* 1999; Decaestecker *et al.* 2007; Thrall *et al.* 2012; Jousimo *et al.* 2014). Nonetheless, we still know surprisingly little about the genetics of the co-evolutionary process.

In order to understand how co-evolutionary dynamics are generated and how this gives rise to patterns in adaptation across populations, it is necessary to characterize interactions between specific parasite exploitation genes and host defence genes (Gandon *et al.* 2008; Thompson 2009). Indeed, the importance of host–parasite interaction genetics has long been recognized, starting with classic concepts in plant pathology (Flor 1956). Interaction genetics define 'who attacks/resists whom' in a population, thereby determining the range and specificity of genotypes involved in the interaction. There are two broad families of genetic architecture models characterizing the structure of host–parasite bipartite interaction networks. Gene-for-gene (GFG) interactions hypothesize that the parasite has an infection locus that overcomes the value of the corresponding host resistance locus. In contrast, matching allele models (MA) assume that infection requires an exact qualitative match between the host and parasite types. Most evidence linking putative genetic interactions to co-evolutionary dynamics comes from experimental evolution of bacteria and phage (e.g. Hall *et al.* 2011b; Tack *et al.* 2012; Brockhurst & Koskella 2013; Betts *et al.* 2014) and a small number of field studies (Dybdahl & Lively 1998; Enjalbert *et al.* 2005; Mboup *et al.* 2012; Thrall *et al.* 2012).

Interaction genetics have been studied in various natural systems by establishing genotype-by-genotype (GxG) interaction matrices in controlled infection experiments (e.g. Thompson & Burdon 1992; Carius *et al.* 2001; Kaltz & Shykoff 2002; Poullain *et al.* 2008). However, apart from detecting statistically significant genetic interactions, results have generally remained inconclusive regarding the structure of the interaction matrix and how these interactions affect the co-evolutionary process (Frank 1994, 1996; Parker 1994). Recently, several studies have employed tools from community ecology to analyse GxG interactions as bipartite networks (e.g. Poisot *et al.* 2011b; Beckett & Williams 2013; Weitz *et al.* 2013). Bipartite networks between antagonists can

be classified as random, nested, modular or one-to-one (e.g. Newman 2006; Liu & Murata 2009; Ulrich 2009; Weitz *et al.* 2013). In this terminology, GFG interactions can generate networks with all-infectious (or all-resistant) generalist types leading to a nested structure. In contrast, MA should produce networks of high specificity composed of infection and resistance specialists and a more modular structure (Weitz *et al.* 2013; Fig. S1, Supporting information). Furthermore, multiple genes may be involved in a co-evolutionary interaction (Frank 1996; Agrawal & Lively 2003; Thrall *et al.* 2015), may act simultaneously or sequentially (two-step infection) and each involve either MA or GFG interactions, possibly associated with different fitness costs (Agrawal & Lively 2003). As a result, the 'realized' network structure may be neither perfectly modular nor perfectly nested. The involvement of multiple genes may also produce a multiscale network structure; for example, it has been suggested that larger taxonomic groups have MA relationships, and within these groups, interactions are closer to GFG (Beckett & Williams 2013; Flores *et al.* 2013). This gives rise to networks in which modules show an internally nested structure (Weitz *et al.* 2013).

Despite a growing understanding of how interaction genetics produces network structure and co-evolutionary dynamics, we currently lack a formal framework for how the latter two are linked. Such associations not only reflect the current and recent past states of the co-evolutionary process, but also how network structure is predictive of future co-evolutionary dynamics. For instance, work on bacteria–phage systems indicates that molecular evolution at interaction loci underlies contemporaneous co-evolutionary change (Paterson *et al.* 2010; Scanlan *et al.* 2011, 2015). Indeed, theory predicts associations between interaction genetics and the type of co-evolutionary dynamics (e.g. Thompson & Burdon 1992; Frank 1996; Agrawal & Lively 2003). Namely, under GFG, we can expect cumulative selective sweeps of host and parasite genes (so-called arms race dynamics; hereafter ARD), with ever-increasing attack and resistance ranges. In contrast, MA interaction genetics should allow frequency-dependent cycling of host and parasite genes over time (Red Queen or, more generally, fluctuating selection dynamics; hereafter FSD). However, certain GFG-type systems may show FSD (e.g. Sasaki 2000), suggesting that the basic structure of interaction matrices needs to be characterized in sufficient detail in order to explain co-evolutionary dynamics.

Because species almost invariably interact in spatially structured environments, understanding how genetic interactions produce and are, in turn, affected by co-evolutionary mosaics is important in understanding diversity and adaptation (Thompson 2005). Local

adaptation in particular is central to determining how species evolve to one another. A geographic pattern of local adaptation is a direct consequence of one player adapting to the locally most common genotype(s) of its opponent. This is particularly true if the acquisition of the necessary genes trades off with the performance on foreign (allopatric) antagonists. One general, straightforward prediction is that the player with the higher evolutionary potential should be locally adapted to its opponent, due to a higher capacity to sample and adapt to local genotypes before they counteradapt. Evolutionary capacity is expected to increase with higher mutation rate or increased migration rate, shorter generation time, greater trait change or lower adaptive trait costs (Gandon 2002; Nuismer & Gandon 2008; Gandon & Nuismer 2009). Despite both laboratory and field assessments of local adaptation and driving ecological factors (reviews and meta-analyses in Kaltz & Shykoff 1998; Greischar & Koskella 2007; Hoeksema & Forde 2008; Brockhurst & Koskella 2013; Koskella & Brockhurst 2014), in particular in systems of bacteria and their phage predators (Forde *et al.* 2004; Morgan *et al.* 2005; Morgan & Buckling 2006; Koskella *et al.* 2011), only scant investigation has actually established a molecular basis for trait interactions and how they may scale up to population-level patterns (Perry *et al.* 2015).

To the best of our knowledge, no study has attempted to establish an integrated approach, combining a molecular basis for trait interactions with the structure of these interactions in bipartite networks, and link these to the larger-scale patterns of co-evolutionary dynamics and local adaptation. We take initial steps towards this challenge by investigating network structure, its change and local adaptation in co-evolving populations of the Gram-negative bacterium *Pseudomonas aeruginosa* (PAO1) and two lytic phage isolates. Previously, Betts *et al.* (2014) used time-shift assays to show that the phage 14-1 (Myoviridae) exhibited arms race type co-evolutionary dynamics, whereas LUZ19 (Podoviridae) showed fluctuating selection dynamics with the same *P. aeruginosa* strain over the course of 10 serial transfers (approximately 60 bacterial generations). We qualitatively assessed the prediction that parasite adaptation in arms race systems involves increases in infectivity ranges and should therefore result in more nested local network structures. In contrast, we hypothesize that fluctuating selection dynamics should lead to a less nested network and possibly even a modular network structure, the latter characterized by the presence of specialist phage and bacteria with more restricted attack and defence ranges. We further evaluated the prediction that, all else being equal, increased host range within populations should be positively correlated with levels of parasite local adaptation between

populations. A final prediction concerns how co-evolutionary dynamics are expected to associate with local adaptation. Several studies have indicated that endogenous or exogenous processes that create co-evolutionary differences or asynchrony between populations (e.g. differential migration, drift, isolation by distance, multiple interaction genes, different habitat characteristics) potentially foster patterns in local adaptation (e.g. Lively 1999; Hochberg & Møller 2001; Gandon 2002; Nuismer 2006; Gandon & Nuismer 2009). Gandon & Nuismer (2009) compared and contrasted matching allele models with gene-for-gene models, the former tending to generate FSD more than the latter. They found a tendency for matching allele models to produce more local adaptation than gene-for-gene models, but this observation depended importantly on underlying model assumptions and specific values assigned to parameters.

To track evolutionary change in network structure, we isolated single phages and single bacteria from each population at three time points during the long-term experiment of Betts *et al.* (2014). We then performed cross-infection assays to quantify their resistance and infection ranges. From these data, we constructed phage–bacteria infection networks. We compared the structure (nestedness and modularity) of each of these networks, their mean impact and host range over time and between the two phages. To measure local adaptation, we performed cross-infection assays between bacteria and phage from different populations. Finally, we sequenced bacterial receptor genes for evidence of molecular evolution underlying the observed local differentiation, namely the evolution of restricted vulnerability and associated network structure.

Methods

Culture media and conditions

Unless otherwise stated, all experiments were conducted in King's B (KB) culture medium (King *et al.* 1954). Bacterial cultures were introduced into 30-mL plastic Falcon tubes (microcosms) containing 5 mL of KB, incubated at 37 °C and 200 rpm orbital agitation. For pairwise infection assays, we used Thermo Scientific™ Nunc™ MicroWell™ 96-Well Microplates, incubated at 37 °C without agitation.

Isolation of bacterial and phage clones

We employed previously frozen samples (replicates stored at −80 °C in 25% glycerol) corresponding to the beginning, the middle and the end of the experiment (transfers 1, 5 and 9; hereafter T1, T5 and T9) from

bacterial populations co-evolving with each of two different phage lines (14-1 and LUZ19) from the study of Betts *et al.* (2014). The study of Betts *et al.* (2014) employed 20 arbitrarily selected bacterial isolates from multiple time points and confronted each with a sample of the sympatric phage population (which would have potentially contained numerous clones). The clones employed in the present study were arbitrarily sampled from these same populations and thus are unlikely to be 100% identical to those isolated by Betts *et al.* (2014).

Samples were incubated overnight in 5 mL KB at 37 °C in an orbital agitator at 200 rpm (intermittent agitation, 1 min every 30 min). The overnight-incubated samples were then centrifuged at 13 000 *g* for 5 min to separate bacteria and phage; the supernatant was stored at 4 °C as the whole phage population, while the pelleted bacteria was resuspended and streaked on to KB agar plates and incubated again overnight. Twelve bacterial colonies were then chosen arbitrarily from the incubated plates and used to initiate 12 separate microcosms. After overnight incubation of these microcosms, a sample from each was stored at −80 °C in 25% glycerol for subsequent infection assays, while the remaining culture was used for the second phase of phage amplification. In total, we isolated 18 groups of 12 bacterial clones (2 phages × 3 replicate populations × 3 time points).

Figure S2 (Supporting information) presents an overview of the isolation method. In order to limit the network to phage clones that could interact with at least one of the 12 bacterial clones isolated from the same population, each phage was amplified on a master population of the 12 isolated sympatric bacterial clones (as prepared above) with each contributing bacterial clone introduced at an equal volume (8.3 μL) and an optical density (OD) of 0.0083 at 600 nm (total OD of 0.1). The mix was then incubated for 6 h at 37 °C, whereupon 10 μL of the phage extracted from the stored evolution experiment was added, and the resulting microcosm was incubated overnight (18 h at 37 °C with 200 rpm intermittent orbital agitation). The amplified phages were then isolated from the mix by centrifuging at 13 000 *g* for 5 min, removing the pellet and adding 10% v/v of chloroform to kill the remaining bacteria. The sample was then serially diluted to the point where phage plaques (PFUs) could be counted; 10 μL droplets of the resulting dilutions were administered on a lawn of the ancestor bacteria on soft-top KB agar to isolate single PFUs; 12 phage plaques from each plate were then arbitrarily chosen and amplified separately on the ancestor bacteria to produce 12 single phage clones from each original population. Each phage clone was then titrated so that an equal density could be administered in the infection assays (500 pfu/mL).

Pairwise infection protocol

We tested the impact of each phage isolate by introducing 10 μL of the phage sample into 96-well plates, each well containing 190 μL of sympatric bacteria, previously corrected to an OD of 0.1 at 600 nm (minimum readable level), using a BMG Clariostar™. Due to large sample numbers and time constraints, the plates were incubated for a restricted time window of 6 h (37 °C without agitation) and then their ODs were measured.

Network analyses

For network indices, we used only significant interaction between single bacterial and phage isolates, as measured by impact (see below for methodology). However, the network analysis only used whether an impact occurred and not its strength. We focused on two network indices, nestedness and modularity (see Fig. S1, Supporting information), which were estimated using R 3.3.2 (packages *bipartite*, *vegan*, *plyr* and *ggplot2*; R Core Team 2015). We used the overlap and decreasing fill (NODF) index to estimate the nestedness of our networks (Almeida-Neto *et al.* 2008; Ulrich 2009). A NODF value of 1 corresponds to a maximally nested network, while a value of 0 indicates that the matrix is empty. We used the *computemodules* routine from the R bipartite package to measure modularity (Dormann *et al.* 2008), which makes use of Newman's modularity measure (Newman 2004). Modularity ranges from 0 to 1 on adequately sized networks, with lower values representing lower modularity and 1 being maximally modular.

To test whether nestedness and modularity estimates for a given network were significantly different from random, the values were compared to a null model that kept the same number of links as the original matrices, but randomly reshuffled the links between the host and the phage isolates. This model was used to construct one hundred random matrices for each of our eighteen matrices (a total of 1800 matrices). We then compared the values of nestedness and modularity for each matrix to the mean and variance of nestedness and modularity for its random counterparts. The difference was considered significant if the actual value occurred outside the 95% central values of the random matrices.

Furthermore, as expected, modularity was negatively correlated with the number of interactions per network ($r = -0.82$, $n = 18$, $P < 0.0001$, across all networks), and nestedness positively correlated ($r = 0.57$, $n = 18$, $P = 0.0129$). Therefore, to make networks with different numbers of interactions comparable, we regressed modularity and nestedness on the number of interactions per network and extracted the residuals from all

regressions (including each of the 100 randomly redistributed networks). These residual estimates allow comparisons of different networks, once the differences in the number of positive interactions have been taken into account.

Estimating mean phage impact and host range

The impact of each phage isolate j on each bacterial isolate i was measured assuming that changes in optical density sufficiently correlated with phage fitness $M_{i,j}$ (Lenski & Levin 1985; Poisot *et al.* 2013) such that

$$M_{i,j} = 1 - \ln(OD_{i,j,6}/OD_{i,j,0})/\ln(OD_{i,6}/OD_{i,0}), \quad (1)$$

where $OD_{i,j,6}$ ($OD_{i,6}$) refers to the optical density of bacteria i in the presence (absence) of phage j after 6 h.

To determine whether a phage had a significant interaction with its host (i.e. $M_{i,j}$ is significantly larger than 0), the difference in the mean optical density in the presence ($OD_{i,j,6} - OD_{i,j,0}$) and absence ($OD_{i,6} - OD_{i,0}$) of the phage was statistically compared using Dunnett's test. A statistically significant reduction in optical density was considered to be evidence for the phage having an interaction with the (host) bacterium. The host range of a given phage R_j is the number of bacterial isolates on which the phage had a significant impact. The mean impact of a given phage I_j is the sum of its significant impacts on all its hosts divided by its range $I_j = M_j/R_j$.

We used linear mixed models to investigate variation in residual nestedness, residual modularity, phage host range and phage impact. Statistical models contained phage type (14-1, LUZ19) and replicate population (nested within phage type) as explanatory factors, and time point as a covariate (transfers 1, 5 and 9). Initial full models (including interactions with time point) were reduced using backward model simplification (where nonsignificant terms are sequentially removed from full model, starting with highest-order interactions). Data sets for nestedness and modularity contained one data point per network ($n = 18$); in the same way, values of host range and impact were averaged over the 12 phages per network prior to analysis. For each network, we further analysed genetic correlations between host range and phage impact (averaged over the different bacterial clones), using the values obtained for the 12 phages in each network (i.e. $n = 12$ for each correlation).

Local adaptation

For a local adaptation assay, we combined the 12 single isolates of phages for each population into a single mix.

The same procedure was applied to bacteria from each population. Each population of bacteria was grown without phage in 5 mL of KB for 6 h with agitation, after which the OD was corrected to the lowest common denominator of 0.4 (at 600 nm) with three replicates for each interaction with a given phage network population. Each bacterial network population mix was then exposed under the same experimental conditions to each of the network phage population mixes (all possible combinations among three replicate networks for each phage type at T9: 2 phage types × 3 bacterial populations × 3 phage populations × 3 replicates = 54 replicates). The OD after 18 h was measured and compared against the (control) line without any phages. Phage impact was calculated using equation 1; in contrast to the network analyses, nonsignificant interactions were included, as they may indicate maladaptation.

Signals of local adaptation were investigated separately for the two phages by constructing a statistical model with phage impact as the response variable and bacterial population and phage population as explanatory factors. The variation explained by the bacteria × phage population interaction was then decomposed to test for a difference between sympatric and allopatric combinations (see Kaltz *et al.* 1999). To assess the relationships between local adaptation and our different network parameters, we calculated the mean difference between sympatric and allopatric phage impact for each of the six replicate populations and tested for correlations with estimates of residual nestedness, residual modularity, total host range and phage impact, as measured for T9.

Genetic analysis

Recent work (Betts *et al.* 2016) identified bacterial genes in which mutations can confer resistance to the two phages used in this study, *wzy* (involved in LPS biosynthesis) for phage 14-1 and *pilF* (involved in type IV pili formation) for phage LUZ19. We examined the sequence of these genes in their respective treatments at T9. For each of the nine replicate lines, three representative bacterial clones were chosen, the most resistant, the closest to the mid resistant and the least resistant, as measured by the mean phage impact on these clones in their corresponding network tests (18 bacterial clones in total). Genomic DNA from each bacterial clone was obtained by choosing a single bacterial colony and then incubating it at 95 °C for 30 min in molecular-grade water. Regions for sequencing were amplified by PCR (Table S1, Supporting information). PCR samples were sequenced by Eurofin on ABI 3730XL sequencers. ACT Artemis was used to compare evolved strains to the ancestor.

Results

Nestedness and modularity

We found a high number of unique interactions within each network (a mean of 84% and 86% for 14-1 and LUZ19, respectively; Table S2, Supporting information), suggesting that the majority of the isolates differed genetically at interaction loci. Overall, the majority of the phage–bacteria networks displayed a nested pattern (mean = 0.71 ± 0.03 SE, $n = 18$) and had low values of modularity (mean = 0.18 ± 0.02 SE, $n = 18$). Figure 1 shows the full-sorted networks of bacterial populations co-evolving with phages 14-1 and LUZ19, respectively (see Fig. S3, Supporting information for the binary representation used in our analyses). In comparison with randomly simulated networks (with the same number of positive interactions), 14 of the total 18 observed networks had significantly higher nestedness levels than expected by chance (outside the bar of 95% percentile range in Fig. 2), and 16 networks were significantly less modular than random networks (Fig. 2). Overall, modularity and nestedness were negatively correlated (all populations and time points combined: $r = -0.70$, $n = 18$, $P < 0.0013$).

We had expected more nested networks to emerge for populations co-evolving with the ARD phage (14-1), and more modular networks for populations co-evolving with the FSD phage (LUZ19). However, there was little evidence for such divergent trajectories. Neither residual nestedness nor residual modularity showed significant overall trends through time ($F_{1,11} > 0.2$, n.s.; Fig. 2). There also was no obvious signal of network identity: indices did not significantly differ between the two phages nor among individual replicate populations (all $P > 0.18$), and their interactions with time were also nonsignificant (all $P > 0.5$).

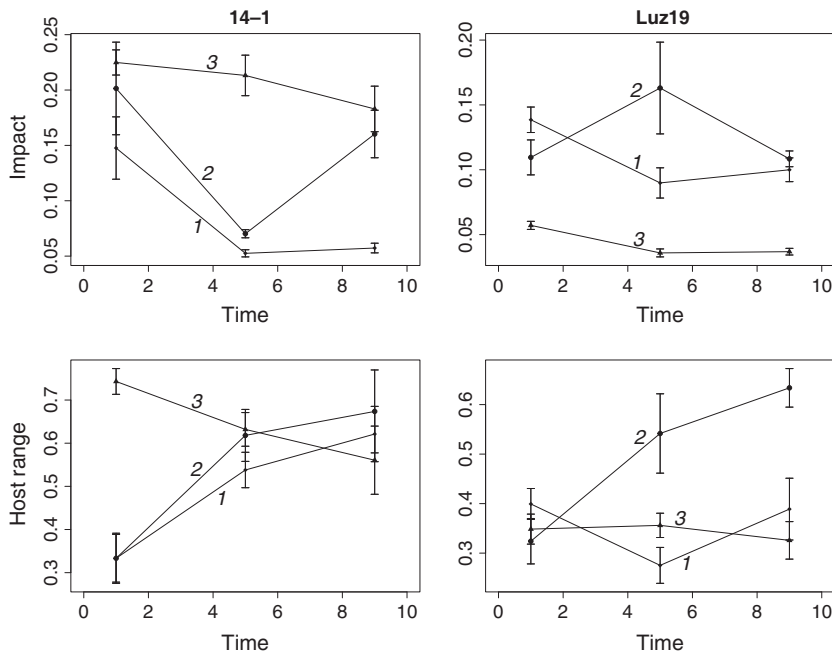### Host range and phage impact

Following the predictions above for network trajectories, we also expected the two phages to differ in their host range evolution. We found variable trajectories in changes in host range among individual replicate populations (Fig. 3), but no clear overall difference between 14-1 and LUZ19 phage populations. Thus, over time, host range increased strongly in some populations, but remained low or even decreased in others (replicate population × time interaction: $F_{4,6} = 5.32$, $P = 0.0355$; phage × time interaction: $F_{1,6} = 0.21$, $P > 0.6$). Over all
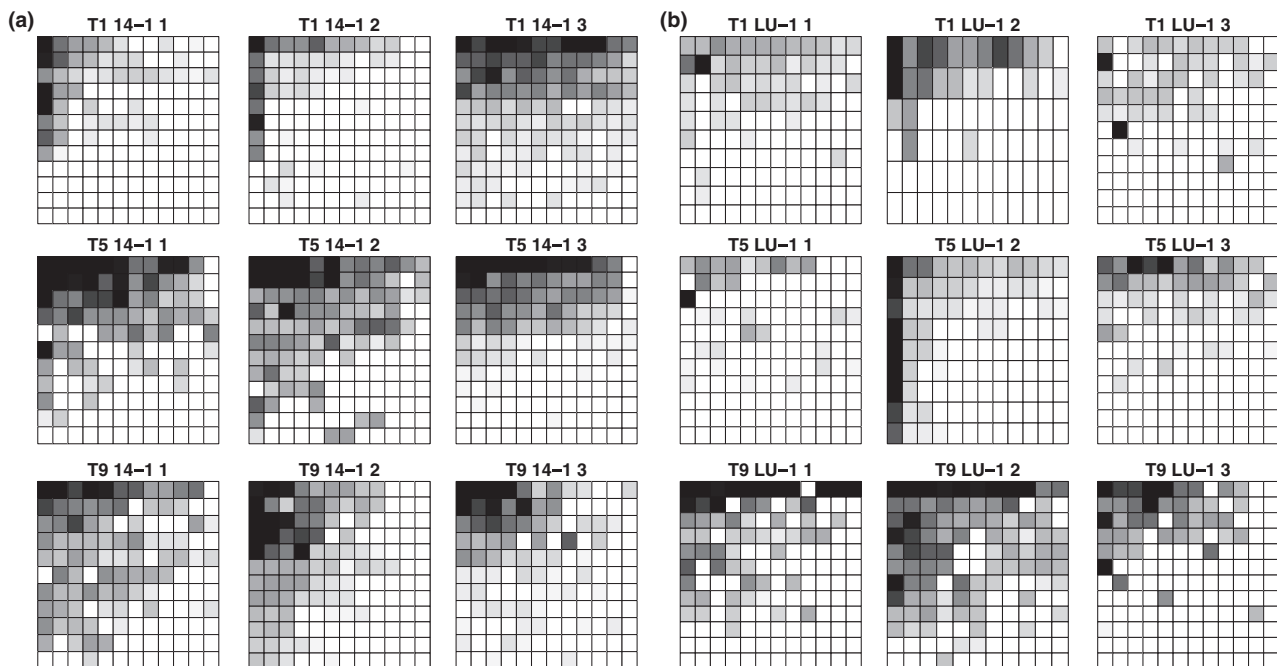
Fig. 1 Networks are nested for both phage types. Networks produced from 12 clones of (a) phage 14-1 and 12 clones of (b) LUZ19, interacting with each of 12 clones of sympatric bacteria from each sampled microcosm. 12 by 12 networks (rows in each network represent bacteria and columns are phages) are evaluated for phage impact at each of three time points (top row = transfer 1; middle row = transfer 5; bottom row = transfer 9), and for three replicates (columns) for each phage type. Each square within each network shows a confrontation between a bacterial clone and a phage clone from a given microcosm. Darker shades of each square indicate a higher impact of phage on the target bacterial clone's OD. Each shade was determined by the maximal impact value for each network with black being set to the maximum and white being 0.
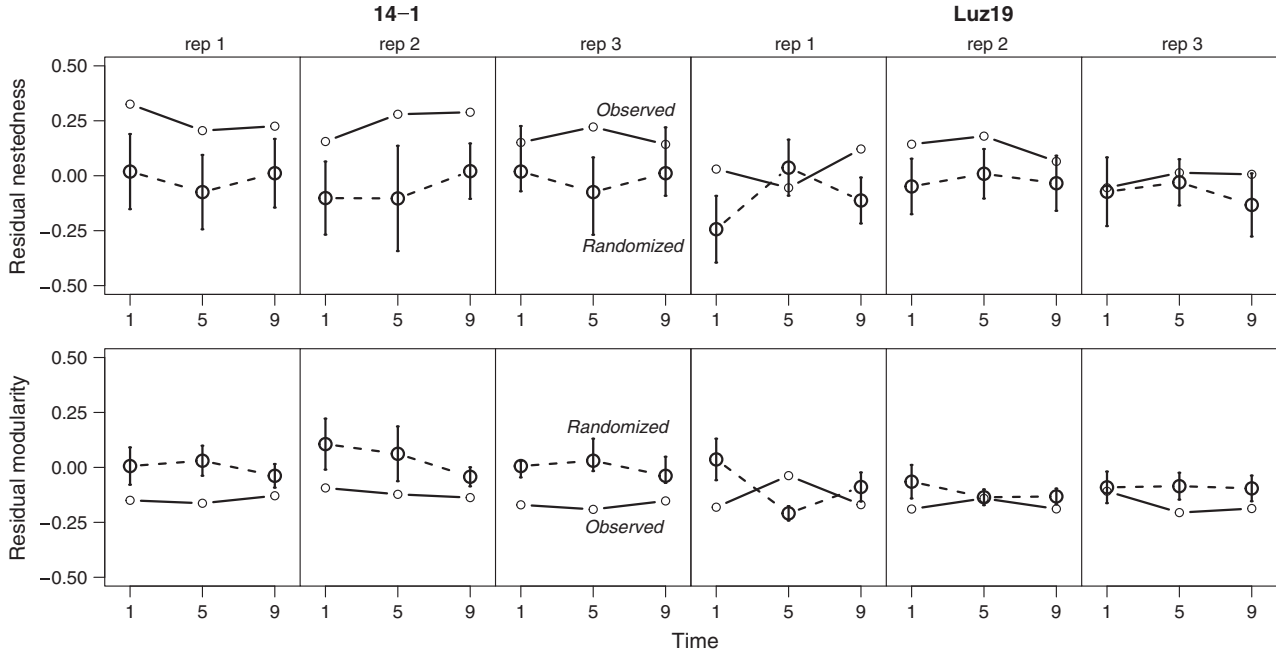
Fig. 2 Statistical inference of network nestedness and modularity. The observed values of nestedness and modularity (solid lines) from the interaction networks were compared to 100 randomly generated networks (stippled lines) for each time point and each phage type. All values were corrected for variation in the number of positive interactions in each network, and hence, residual values are shown. Error bars denote 95% percentile range based on the 100 randomizations. See text for further details.

Fig. 3 Host range increases in some populations, while phage impact tends to decrease over the course of the experiment. Host range is the number of bacterial clones on which a given phage isolate has a significant negative impact on growth. Impact is the quantitative reduction in bacterial growth. Numbers attached to lines indicate population identity. Bars indicate SEs.

time points, host range tended to be larger for the 14-1 phage than for LUZ19 phage, but this trend was not statistically significant ($F_{1,4} = 5.60$, $P = 0.0772$).

Phage impact was measured to test for possible associations (costs) with host range. We found that impact did not significantly vary with phage type (main effect and interaction with time, both $P > 0.2$). We further detected a general decreasing, but non-significant, trend through time ($F_{1,11} = 3.47$, $P = 0.0894$; Fig. 3). Thus, at least for some

populations, temporal increases in host range were associated with decreases in the capacity to reduce host density, which suggests a trade-off between the two quantities. However, analysis of the genetic correlations within populations revealed little evidence for such a trade-off: of the 18 correlations based on the 12 phage isolates from each population and time point, 14 were positive (six with $P < 0.01$) and only four negative (Fig. S4; Table S3, Supporting information). Generally, the genetic correlations remained positive or became positive over time (T1, T5 and T9; Fig. S5), indicating that phage variants with larger host range also had larger impacts on host density. Only one LUZ19 replicate population showed an increasing negative correlation, consistent with a trade-off between host range and impact. We obtained very similar results when using summed impact over all hosts (not shown), rather than mean impact, again suggesting that increased range generally does not come at a cost.

Local adaptation

We further tested whether network structure might scale up to the between-population-level patterns of local adaptation. We found a consistent pattern of local adaptation of phage 14-1 to its hosts ($F_{1,3} = 16.54$, $P = 0.0268$), as indicated by stronger phage impact in sympatric bacteria–phage combinations than in allopatric combinations. This pattern holds for all three populations tested (Fig. 4). In contrast, no clear general pattern of local adaptation was detected for phage LUZ19 ($F_{1,3} = 8.25$, $P > 0.06$). Combining data over all six tested replicate populations, we found no indication of a quantitative relationship between the degree of local parasite adaptation and the above network parameters (residual nestedness, residual modularity, host range, phage impact: all

$r \leq 0.2$, $n = 6$, $P > 0.7$; Fig. S6, Supporting information).

Molecular evolution

The sequence analysis showed several mutations for the *wzy* gene from bacteria co-evolving with the 14-1 phage, whereas the *pilF* gene from bacteria co-evolving with the LUZ19 phage showed limited changes, which were mostly large-scale deletions of the upstream region of the gene, or truncation within the gene (Table 1). The mutations observed in the *wzy* gene were typically around the same positions, notably the 290-bp region $\pm$ 9 for four mutations, the 530-bp region $\pm$ 5 for two mutations and the 775-bp region $\pm$ 7 for three mutations. There was also sign of some accumulation of these SNPs, such that, at least in some cases, higher levels of phenotypic resistance were associated with the presence of additional mutations (Table 1). Bacteria that co-evolved with LUZ19 showed no such accumulation, and deletions did not appear representative of position in terms of resistance to LUZ19, with only one of the most resistant isolates having a deletion in the *pilF* gene.

Discussion

Our goal was to determine whether arms race and fluctuating selection co-evolutionary systems produced characteristic genotype-by-genotype interactions, revealed by bipartite network structure and local adaptation. Contrary to expectation, we found that both the ARD (14-1) and FSD (LUZ19) phages produced nested bipartite networks and that only the ARD phage showed a significant level of local adaptation. We also identified mutated receptor genes on bacteria that evolved with phage 14-1, but found no clear signal of evolution in one of the putative receptor genes
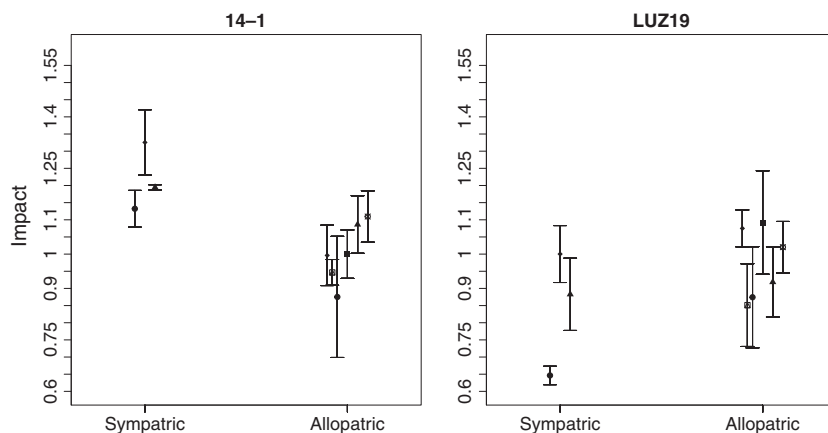
Fig. 4 Local adaptation of the phage. The impact of phage on bacterial growth in allopatric vs. sympatric combinations of bacteria and phage 14-1 or phage LUZ19, measured at T9. For each phage type, all 3×3 combinations between three replicate populations were tested. Each bacterial (phage) population consisted of the mix of all 12 individual bacterial (phage) clones. Each point is the mean value for a different combination of bacterial and phage population (sympatric or allopatric). Error bars denote SEs.

Table 1 Mutations found in the sequenced *wzy* and *pilF* gene in bacteria co-evolved with the phage 14-1 and LUZ19, respectively

Strain network position and replicate population ID	*wzy* Mutations in bacteria co-evolved with 14-1 (& amino acid change)	*pilF* Mutations in bacteria co-evolved with LUZ19
Least resistant 1	Frameshift 776 ΔG (multiple)	Nil
Mean resistant 1	SNP 533 G-A (R-K)	Sequence truncated 641-759
Most resistant 1	SNP 299 G-A (D-N)	Nil
Least resistant 2	Nil	Nil
Mean resistant 2	Frameshift 782 ΔT (multiple)	Upstream deletion bp 1-87
Most resistant 2	Frameshift 782 ΔT (multiple)	Upstream deletion bp 1-197
Least resistant 3	SNP 281 (S-Y)	Nil
Mean resistant 3	SNP 281, 872 (S-Y, V-G)	Upstream deletion bp 1-316
Most resistant 3	Frameshift 420 ΔT (multiple)	Nil

Three representative isolates were picked from each of the three replicate populations at time point 9 (total of nine colonies from each phage population). Their selection was based on their level of resistance (measured as the inverse of impact $M_{i,j}$) to their co-evolved network phages. Comparisons with the ancestral strain of *Pseudomonas aeruginosa* PAO1 showed multiple nonsynonymous SNPs and frameshift mutations in the *wzy* gene. These changes potentially impact on the structure of the LPS, the receptor for the phage 14-1 and expression of the type IV pili. For *pilF*, we found large-scale deletions of the upstream region of the gene, truncation within the gene or no change at all.

associated with infection by LUZ19. These results, although not contradicting theoretical predictions, suggest that the ecological and evolutionary processes contributing to larger-scale patterns are complex. We discuss our main findings below.

Nestedness and modularity

Weitz *et al.* (2013) suggested that underlying co-evolutionary interactions could influence network structure. A nested pattern indicates that one or a small number of qualitatively similar resistance (host) and infectivity (parasite) genotypes dominate the co-evolutionary process and that less frequent types are either decreasing towards extinction (lower relative fitness) or increasing in frequency (higher relative fitness) to eventually displace the most abundant types (e.g. Gomulkiewicz *et al.* 2000; Nuismer & Thompson 2006; Beckett & Williams 2013). We found that nested networks evolved repeatedly and consistently in independent replicate microcosms. We had expected such nested networks for phage 14-1, as it had shown a predominantly ARD pattern in the experiment (Betts *et al.* 2014). However, despite substantial differences in their co-evolutionary dynamics (Betts *et al.* 2014), networks with both ARD (phage 14-1) and FSD (phage LUZ19) phages showed similar levels of high nestedness and nonmodularity. These patterns are consistent with the majority of reported phage–bacteria systems (Flores *et al.* 2011) and were robust over evolutionary time during the experiment.

In contrast to nested matrices, modular networks do not necessarily have single-most infectious or resistant types and could therefore be associated with sustained frequency-dependent selection. Thus, we had expected relatively more modular networks for the LUZ19 phage type, reflecting their fluctuating selection co-evolutionary dynamics (Betts *et al.* 2014). However, our analyses show that the majority of networks were not significantly modular (Fig. 2). Previous study (Poisot *et al.* 2011b, 2013) suggests that our sampling of 12 host and 12 parasite genotypes should have been sufficient to represent each network, including the potential detection of a signal of modularity. Given the findings from field populations of fluorescent pseudomonas and infective lytic phages that networks are both nested and modular (Poisot *et al.* 2013), we suggest that the lack of modularity in our study was due to the source experiments commencing with single bacterial and phage clones, whereas field populations are diversified, probably containing many bacterial species and/or strains, and phage families. It is currently unknown to what extent the communities in the Poisot *et al.*'s (2013) study may have previously co-evolved (as was observed during the course of the experiment in our populations; Betts *et al.* 2014), although other studies in seminatural or natural environments are consistent with the occurrence of phage–bacteria co-evolution (Koskella & Brockhurst 2014).

Host range and Impact

Under pure ARD co-evolution, the accumulation of infectivity alleles should lead to an ever-increasing host range (and consequently, nested networks). However, it is likely that this accumulation is not indefinite and that, at some point, increasing host range bears fitness costs. Importantly, such a cost of generalism may

prevent the fixation of large-range variants in putative gene-for-gene systems and produce FSD dynamics (Sasaki 2000; Hall *et al.* 2011b). Examples can be found in plant–pathogen systems, where so-called costs of virulence may lead to the selective elimination of unnecessary infectivity alleles and promote their frequency-dependent cycling (Van der Plank 1968; Bahri *et al.* 2009). Such costs of infectivity alleles may explain our finding of a nested network structure for LUZ19, despite our previous observation of FSD coevolution (Betts *et al.* 2014).

We investigated possible costs of generalism by quantifying changes in host range and its relationship with phage impact (i.e. the capacity to reduce host density as measured by decreases in optical density). We found that, unlike for modularity and nestedness, populations showed more divergent trajectories for host range. Thus, while the topography of links in the network remained relatively constant through time, the total number of links (i.e. host range) strongly increased in some populations, consistent with ARD-like co-evolution and concomitant increases in infectivity range (Poullain *et al.* 2008; Hall *et al.* 2011a; Betts *et al.* 2014). Also consistent with ARD, we observed mostly strong positive genetic correlations between host range and phage impact within networks of the 14-1 phage. Therefore, selection for increasing host range did not appear to be constrained by a fitness cost with respect to the capacity to reduce host density. This is in agreement with similar relationships for field populations of fluorescent pseudomonads by Poisot *et al.* (2013). However, for the FSD phage LUZ19 and contrary to our prediction, we found no clear evidence for a cost of generalism. Only one of the three replicate populations developed a trade-off between range and impact, compatible with costs and a FSD co-evolution scenario.

Molecular evolution

Consistent with molecular evolution in bacterial receptors due to phage selection (Betts *et al.* 2016), we detected mutations and frameshifts in the samples of *Pseudomonas aeruginosa* exposed to phage 14-1 as well as upstream deletions covering the start region of the gene and sequence truncations in bacteria exposed to LUZ19. Namely, we observed several mutations in the *wzy* gene, including parallel evolution of similar SNPs, which may have reduced the efficiency of phage adsorption. Mutations in *wzy* can affect B-band LPS biosynthesis in *P. aeruginosa*, altering LPS structure or even leading to absent LPS structures on the bacterial surface (Islam *et al.* 2010). Moreover, the gene *wzy* has previously been highlighted as a focus of 14-1 imposed selection, and SNPs in *wzy* can confer resistance to both 14-1 and other LPS-dependent phage (Betts *et al.* 2016). Although there is indication of the same genetic signature associated with the least and intermediate vulnerable bacterial clones in one of the 14-1 networks, we were not able to statistically determine a signal of association with resistance phenotypes and sequenced genotypes. Moreover, many other genes influence LPS, meaning that the mutations identified here may only be a subset of changes that actually occurred.

For bacteria co-evolving with phage LUZ19, analysis of sequences of the *pilF* gene revealed limited evidence of type IV pili evolution, contrasting with the findings by Betts *et al.* (2016). These discrepancies, however, may be explained by genes not sequenced in our study (such as *pilI* and *pilH*), yet directly involved in the production of type IV pili. We therefore urge caution in interpreting these preliminary molecular findings.

Local adaptation

The classic view of host–parasite co-evolution is that parasites have a higher evolutionary potential than their hosts, due to their shorter generation time and larger population sizes (Haldane 1949; Hamilton 1980). Faster parasite adaptation than host counteradaptation is thus expected to translate into a geographic pattern of locally adapted parasites. Over the past two decades, a large body of research has explored the various ecological and evolutionary processes affecting patterns in local (mal)adaptation of host and/or parasite, namely differential migration or habitat productivity (Gandon *et al.* 1996; Lively 1999; Gomulkiewicz *et al.* 2000; Hochberg & Møller 2001; Gandon 2002; Gandon & Michalakis 2002; Morgan *et al.* 2005; Morgan & Buckling 2006; Nuismer 2006; Nuismer & Gandon 2008; Gandon & Nuismer 2009). In the limiting situation considered in our experiment of isolated populations and controlled environmental conditions, one of our two phages (14-1) matched the classic prediction of local parasite adaptation. Interestingly, under similar experimental protocols, a related bacterium (*P. fluorescens* SBW25) often produces the opposite pattern of parasite maladaptation (Buckling & Rainey 2002; Morgan *et al.* 2005; but see Duncan *et al.* 2016). The mechanisms explaining these contrasting findings remain to be elucidated.

Based on what little theory exists, we hypothesized that the FSD phage LUZ19 should be more likely to produce patterns of local adaptation than the ARD phage 14-1. This prediction was not met, and moreover, we found no corresponding scaling-up of network characteristics. Namely, levels of modularity (which should be associated with FSD dynamics) were uncorrelated with levels of local adaptation. Clearly, these correlation tests were based on relatively small number of

populations ($n = 6$), limiting statistical power. This could also explain why we found no support for the general prediction that increasing local host range should be correlated with levels of local adaptation. We suggest that more theoretical work is needed to clarify the relationship between local network structure, co-evolutionary dynamics and ensuing patterns of local adaptation.

Our limited molecular data do not allow a formal analysis of a link between patterns of molecular differentiation and patterns of local adaptation. The available data show different mutations in different populations, contributing to putative bacterial resistance in the 14-1 confronted bacteria. Such among-population differentiation is at least broadly consistent with the emergence of local adaptation. In contrast, we found less indication of *pilF* alteration in the LUZ19-co-evolved bacteria. This preliminary result is consistent with our observations of local adaptation. However, evolution can occur in the same gene for LUZ19 adapted bacteria (Betts *et al.* 2016), and moreover, there are many other candidate genes affecting type IV pili, which could explain the co-evolutionary pattern and lack of local adaptation.

There are methodological differences between the present study and that employed in Betts *et al.* (2014) that could have influenced the results and conclusions. First, the analyses in the present study are based on randomly chosen bacterial clones from frozen samples of Betts *et al.* (2014). Given that the phages in the present study were isolated initially on the ancestral strain, it is possible that they only partially reflect actual phage community composition occurring at each time step in the co-evolutionary study of Betts *et al.* (2014). Moreover, the infectivity assays in our study were based on significant decreases in the OD of bacterial host populations, as opposed to infectivity assays of phage populations on bacterial clones in Betts *et al.* (2014). It is therefore possible that positive infectivity from this previous study was not always associated with statistically significant drops in OD in the present study, but this is impossible to test, because different clones from the same populations may have been sampled in the current study.

Second, our local adaptation assays were performed with the phage isolates that had been shown to infect hosts in the sympatric network. Assuming that phage clones existed at high frequency (i.e. among the highest 12 clones in the source populations) that *did not* infect any of the 12 most frequent bacterial clones, this could have increased the chances of detecting significant signals of local adaptation. However, using a full representative sample of phages (i.e. that infect either local hosts or hosts in the other populations tested) would have introduced another bias in the measure, that is investigating phages that do not infect the 12 chosen bacterial isolates, but *either do or do not* infect others in the sympatric population. Future work is needed to assess the importance of these and other potential biases to our understanding of local adaptation.

Conclusions

Despite previously described differences in the co-evolutionary dynamics between the two phages investigated here, we found the bipartite networks to show similar, highly nested structures. The main properties distinguishing these ARD and FSD phage–bacterial systems are that (i) the ARD phage is locally adapted to its host and based on limited sequencing, (ii) the existence of molecular changes to bacterial receptors after co-evolution with the ARD phage showed SNPs, while co-evolution with the FSD phage sometimes exhibited large-scale truncations of the bacterial receptor. Our study shows that considerable variation emerges between replicates with the same initial bacterial and phage types, indicating that probabilistic events (specific mutations in specific genetic backgrounds) could play an important role in larger-scale co-evolutionary patterns.

Acknowledgements

References

Agrawal A, Lively CM (2002) Infection genetics: gene-for-gene versus matching-alleles models and all points in between. *Evolutionary Ecology Research*, **4**, 79–90.

Agrawal AF, Lively CM (2003) Modelling infection as a two-step process combining gene-for-gene and matching-allele genetics. *Proceedings of the Royal Society of London B: Biological Sciences*, **270**, 323–334.

Almeida-Neto M, Guimarães P, Guimarães PR *et al.* (2008) A consistent metric for nestedness analysis in ecological systems: reconciling concept and measurement. *Oikos*, **117**, 1227–1239.

Ashby B, Gupta S, Buckling A (2014) Spatial structure mitigates fitness costs in host-parasite coevolution. *American Naturalist*, **183**, E64–E74.

Bahri B, Kaltz O, Leconte M *et al.* (2009) Tracking costs of virulence in natural populations of the wheat pathogen, *Puccinia striiformis* f.sp.tritici. *BMC Evolutionary Biology*, **9**, 26.

Beckett SJ, Williams HTP (2013) Coevolutionary diversification creates nested-modular structure in phage-bacteria interaction networks. *Interface Focus*, **3**, 20130033.

Bell G, Graham B, Maynard Smith J (1987) Short-term selection for recombination among mutually antagonistic species. *Nature*, **328**, 66–68.

Betts A, Kaltz O, Hochberg ME (2014) Contrasted coevolutionary dynamics between a bacterial pathogen and its bacteriophages. *Proceedings of the National Academy of Sciences of the United States of America*, **111**, 11109–11114.

Betts A, Gifford DR, MacLean RC, King KC (2016) Parasite diversity drives rapid host dynamics and evolution of resistance in a bacteria-phage system. *Evolution*, **70**, 969–978.

Brockhurst MA, Koskella B (2013) Experimental coevolution of species interactions. *Trends in Ecology & Evolution*, **28**, 367–375.

Buckling A, Rainey PB (2002) Antagonistic coevolution between a bacterium and a bacteriophage. *Proceedings of the Royal Society B: Biological Sciences*, **269**, 931–936.

Carius HJ, Little TJ, Ebert D (2001) Genetic variation in a host-parasite association: potential for coevolution and frequency-dependent selection. *Evolution*, **55**, 1136–1145.

Decaestecker E, Gaba S, Raeymaekers JAM et al. (2007) Host-parasite "Red Queen" dynamics archived in pond sediment. *Nature*, **450**, 870–873.

Dormann CF, Gruber B, Fruend J (2008) Introducing the bipartite package: analysing ecological networks. *R News*, **8**, 8–11.

Duncan AB, Dusi E, Jacob F, Ramsayer J, Hochberg ME, Kaltz O (2016) Hot spots become cold spots: coevolution in variable temperature environments. *Journal of Evolutionary Biology*, **30**, 55–65.

Dybdahl MF, Lively CM (1998) Host-parasite coevolution: evidence for rare advantage and time-lagged selection in a natural population. *Evolution*, **52**, 1057–1066.

Enjalbert J, Duan X, Leconte M, Hovmøller MS, De Vallavieille-Pope C (2005) Genetic evidence of local adaptation of wheat yellow rust (*Puccinia striiformis* f. sp. tritici) within France. *Molecular Ecology*, **14**, 2065–2073.

Fischer O, Schmid-Hempel P (2005) Selection by parasites may increase host recombination frequency. *Biology Letters*, **1**, 193–195.

Flor HH (1956) The complementary genic systems in flax and flax rust. *Advances in Genetics* **8**, 29–54.

Flores CO, Meyer JR, Valverde S et al. (2011) Statistical structure of host-phage interactions. *Proceedings of the National Academy of Sciences of the United States of America*, **108**, E288–E297.

Flores CO, Valverde S, Weitz JS (2013) Multi-scale structure and geographic drivers of cross-infection within marine bacteria and phages. *ISME Journal*, **7**, 520–532.

Forde SE, Thompson JN, Bohannan BJM (2004) Adaptation varies through space and time in a coevolving host–parasitoid interaction. *Nature*, **431**, 841–844.

Frank SA (1994) Recognition and polymorphism in host-parasite genetics. *Philosophical Transactions of the Royal Society of London. Series B, Biological sciences*, **346**, 283–293.

Frank SA (1996) Statistical properties of polymorphism in host —parasite genetics. *Evolutionary Ecology*, **10**, 307–317.

Friman VP, Buckling A (2013) Effects of predation on real-time host-parasite coevolutionary dynamics. *Ecology Letters*, **16**, 39–46.

Gandon S (2002) Local adaptation and the geometry of host–parasite coevolution. *Ecology Letters*, **5**, 246–256.

Gandon S, Michalakis Y (2002) Local adaptation, evolutionary potential and host–parasite coevolution: interactions between migration, mutation, population size and generation time. *Journal of Evolutionary Biology*, **15**, 451–462.

Gandon S, Nuismer SL (2009) Interactions between genetic drift, gene flow, and selection mosaics drive parasite local adaptation. *American Naturalist*, **173**, 212–224.

Gandon S, Capowiez Y, Dubois Y et al. (1996) Local adaptation and gene-for-gene coevolution in a metapopulation model. *Proceedings of the Royal Society of London B: Biological Sciences*, **263**, 1003–1009.

Gandon S, Buckling A, Decaestecker E, Day T (2008) Host-parasite coevolution and patterns of adaptation across time and space. *Journal of Evolutionary Biology*, **21**, 1861–1866.

Gómez P, Ashby B, Buckling A (2015) Population mixing promotes arms race host–parasite coevolution. *Proceedings of the Royal Society of London B: Biological Sciences*, **282**, 20142297.

Gomulkiewicz R, Thompson JN, Holt RD et al. (2000) Hot spots, cold spots, and the geographic mosaic theory of coevolution. *American Naturalist*, **156**, 156–174.

Greischar MA, Koskella B (2007) A synthesis of experimental work on parasite local adaptation. *Ecology Letters*, **10**, 418–434.

Haldane JBS (1949) Disease and evolution. *La Ricerca Scientifica*, **19**(suppl.), 68–76.

Hall AR, Scanlan PD, Buckling A (2011a) Bacteria-phage coevolution and the emergence of generalist pathogens. *American Naturalist*, **177**, 44–53.

Hall AR, Scanlan PD, Morgan AD, Buckling A (2011b) Host-parasite coevolutionary arms races give way to fluctuating selection. *Ecology Letters*, **14**, 635–642.

Hamilton WD (1980) Sex versus non-sex versus parasite. *Oikos*, **35**, 282–290.

Harrison E, Laine A-L, Hietala M, Brockhurst MA (2013) Rapidly fluctuating environments constrain coevolutionary arms races by impeding selective sweeps. *Proceedings. Biological Sciences*, **280**, 20130937.

Hochberg ME, Baalen M (1998) Antagonistic coevolution over productivity gradients. *American Naturalist*, **152**, 620–634.

Hochberg ME, Holt RD (1995) Refuge evolution and the population dynamics of coupled host —parasitoid associations. *Evolutionary Ecology*, **9**, 633–661.

Hochberg ME, Møller AP (2001) Insularity and adaptation in coupled victim–enemy associations. *Journal of Evolutionary Biology*, **14**, 539–551.

Hoeksema JD, Forde SE (2008) A meta-analysis of factors affecting local adaptation between interacting species. *American Naturalist*, **171**, 275–290.

Islam ST, Taylor VL, Qi M, Lam JS (2010) Membrane topology mapping of the O-antigen flippase (Wzx), polymerase (Wzy), and ligase (WaaL) from Pseudomonas aeruginosa PAO1 reveals novel domain architectures. *MBio*, **1**, e00189–10.

Jousimo J, Tack AJM, Ovaskainen O et al. (2014) Disease ecology. Ecological and evolutionary effects of fragmentation on infectious disease dynamics. *Science*, **344**, 1289–1293.

Kaltz O, Shykoff JA (1998) Local adaptation in host–parasite systems. *Heredity*, **81**, 361–370.

Kaltz O, Shykoff JA (2002) Within- and among-population variation in infectivity, latency and spore production in a host-pathogen system. *Journal of Evolutionary Biology*, **15**, 850–860.

Kaltz O, Oliver K, Sylvain G et al. (1999) Local maladaptation in the anther-smut fungus *Microbotryum violaceum* to its host plant silene latifolia: evidence from a cross-inoculation experiment. *Evolution*, **53**, 395.

King EO, Ward MK, Raney DE (1954) Two simple media for the demonstration of pyocyanin and fluorescin. *Journal of Laboratory and Clinical Medicine*, **44**, 301–307.

Koskella B, Brockhurst MA (2014) Bacteria-phage coevolution as a driver of ecological and evolutionary processes in microbial communities. *FEMS Microbiology Reviews*, **38**, 916–931.

Koskella B, Thompson JN, Preston GM, Buckling A (2011) Local biotic environment shapes the spatial scale of bacteriophage adaptation to bacteria. *American Naturalist*, **177**, 440–451.

Lenski RE, Levin BR (1985) Constraints on the coevolution of bacteria and virulent phage: a model, some experiments, and predictions for natural communities. *American Naturalist*, **125**, 585–602.

Liu X, Murata T (2009) Community detection in large-scale bipartite networks. In: *Web Intelligence and Intelligent Agent Technologies, 2009. WI-IAT '09. IEEE/WIC/ACM International Joint Conferences on*. pp. 50–57.

Lively CM (1999) Migration, virulence, and the geographic mosaic of adaptation by parasites. *American Naturalist*, **153**, S34–S47.

Lopez-Pascua L, Buckling A (2008) Increasing productivity accelerates host-parasite coevolution. *Journal of Evolutionary Biology*, **21**, 853–860.

Mboup M, Bahri B, Leconte M *et al.* (2012) Genetic structure and local adaptation of European wheat yellow rust populations: the role of temperature-specific adaptation. *Evolutionary Applications*, **5**, 341–352.

Morgan AD, Buckling A (2006) Relative number of generations of hosts and parasites does not influence parasite local adaptation in coevolving populations of bacteria and phages. *Journal of Evolutionary Biology*, **19**, 1956–1963.

Morgan AD, Gandon S, Buckling A (2005) The effect of migration on local adaptation in a coevolving host–parasite system. *Nature*, **437**, 253–256.

Newman MEJ (2004) Analysis of weighted networks. *Physical Review. E, Statistical, Nonlinear, and Soft Matter Physics*, **70**, 056131.

Newman MEJ (2006) Modularity and community structure in networks. *Proceedings of the National Academy of Sciences of the United States of America*, **103**, 8577–8582.

Nuismer SL (2006) Parasite local adaptation in a geographic mosaic. *Evolution*, **60**, 24–30.

Nuismer SL, Gandon S (2008) Moving beyond common-garden and transplant designs: insight into the causes of local adaptation in species interactions. *American Naturalist*, **171**, 658–668.

Nuismer SL, Thompson JN (2006) Coevolutionary alternation in antagonistic interactions. *Evolution*, **60**, 2207–2217.

Parker MA (1994) Pathogens and sex in plants. *Evolutionary Ecology*, **8**, 560–584.

Paterson S, Steve P, Tom V *et al.* (2010) Antagonistic coevolution accelerates molecular evolution. *Nature*, **464**, 275–278.

Perry EB, Barrick JE, Bohannan BJM (2015) The molecular and genetic basis of repeatable coevolution between *Escherichia coli* and bacteriophage T3 in a laboratory microcosm. *PLoS ONE*, **10**, e0130639.

Poisot T, Thrall PH, Hochberg ME (2011a) Trophic network structure emerges through antagonistic coevolution in temporally varying environments. *Proceedings of the Royal Society of London B*, **279**, 299–308.

Poisot T, Lepennetier G, Martinez E *et al.* (2011b) Resource availability affects the structure of a natural bacteria-bacteriophage community. *Biology Letters*, **7**, 201–204.

Poisot T, Lounnas M, Hochberg ME (2013) The structure of natural microbial enemy-victim networks. *Ecological Processes*, **2**, 13.

Poullain V, Gandon S, Brockhurst MA *et al.* (2008) The evolution of specificity in evolving and coevolving antagonistic interactions between a bacteria and its phage. *Evolution*, **62**, 1–11.

R Core Team (2015) *R: A Language and Environment for Statistical Computing*. R Foundation for Statistical Computing, Vienna, Austria.

Sasaki A (2000) Host-parasite coevolution in a multilocus gene-for-gene system. *Proceedings of the Royal Society of London B: Biological Sciences*, **267**, 2183–2188.

Scanlan PD, Hall AR, Lopez-Pascua LDC, Buckling A (2011) Genetic basis of infectivity evolution in a bacteriophage. *Molecular Ecology*, **20**, 981–989.

Scanlan PD, Hall AR, Blackshields G *et al.* (2015) Coevolution with bacteriophages drives genome-wide host evolution and constrains the acquisition of abiotic-beneficial mutations. *Molecular Biology and Evolution*, **32**, 1425–1435.

Tack A, Thrall PH, Barrett LG (2012) Variation in infectivity and aggressiveness in space and time in wild host–pathogen systems: causes and consequences. *Journal of Evolutionary Biology*, **25**, 1918–1936.

Thompson JN (1999) Specific hypotheses on the geographic mosaic of coevolution. *American Naturalist*, **153**, S1–S14.

Thompson JN (2005) *The Geographic Mosaic of Coevolution*, University of Chicago Press, Chicago.

Thompson JN (2009) The coevolving web of life. *American Naturalist*, **173**, 125–140.

Thompson JN, Burdon JJ (1992) Gene-for-gene coevolution between plants and parasites. *Nature*, **360**, 121–125.

Thrall PH, Laine A-L, Ravensdale M *et al.* (2012) Rapid genetic change underpins antagonistic coevolution in a natural host-pathogen metapopulation. *Ecology Letters*, **15**, 425–435.

Thrall PH, Barrett LG, Dodds PN, Burdon JJ (2015) Epidemiological and evolutionary outcomes in gene-for-gene and matching allele models. *Frontiers in Plant Science*, **6**, 1084.

Ulrich W (2009) Ecological interaction networks: prospects and pitfalls. *Ecological Questions*, **11**, 17–25.

Van der Plank JE (1968) *Disease Resistance in Plants*. Academic Press, New York and London.

Weitz JS, Poisot T, Meyer JR *et al.* (2013) Phage – bacteria infection networks. *Trends in Microbiology*, **21**, 82–91.

Data accessibility

J.G., O.K. and M.E.H. conceived and designed the study. A.B. provided the microbial samples. J.G. and L.A. performed the experiments. J.G., L.A., T.P. and O.K. analysed the data. J.G. and C.G.B. obtained and analysed the genetic sequences. J.G., O.K. and M.E.H. wrote the manuscript, and all authors contributed substantially to revisions. All authors gave final approval for publication.

Supporting information

Additional supporting information may be found in the online version of this article.

Fig. S1 Different types of structures of host-parasite interaction networks.

Fig. S2 The procedure for isolating the phage and bacterial clones from the frozen populations.

Fig. S3 Binary representation of networks.

Fig. S4 Mostly positive genetic correlations between phage host range and mean impact on sensitive bacterial clones.

Fig. S5 Temporal genetic correlations.

Fig. S6 Correlations between parasite local adaptation and local network parameters.

Table S1 Primers used to amplify phage receptor genes.

Table S2 Number of unique interactions in each network, infectotypes are all distinct phage isolates, resistotypes are all distinct bacterial isolates (X) = total possible types.

Table S3 Genetic correlations; all $n = 12$, gray shading = significant after Bonferroni correction.